Check for updates

Three-Dimensional PrGO-Based Sandwich Composites With MoS$_2$ Flowers as Stuffings for Superior Lithium Storage

Yangqiang Zhao[1], Ziying Zhang[1]*, Huizhen Zhang[2], Yangyang Zhou[1], Ying Weng[1] and Shisheng Xiong[3]*

[1] School of Materials Engineering, Shanghai University of Engineering Science, Shanghai, China, [2] School of Management, University of Shanghai for Science and Technology, Shanghai, China, [3] School of Information Science and Engineering, Fudan University, Shanghai, China

Graphene-based MoS$_2$ nanocomposites are expected to be promising anode materials for lithium ion batteries because of their large specific capacity and high conductivity. However, the aggregation of graphene and the weak interaction between the two components hinder their practical application. Inspired by the sandwich structure, novel three-dimensional flower-like MoS$_2$-PrGO sandwich composites were proposed as an advanced anode material for lithium-ion batteries. The separated 2D ultrathin rGO nano-sheets were connected by PEO chains and assembled into a well-organized 3D layered spatial structure, which not only avoids the aggregation of graphene but also accommodates a high mass loading of the micro-scale MoS$_2$ nano-flowers. MoS$_2$ nano-flowers with open architecture deliver large specific area. The rGO interlayers act as a conductive framework, making all flower-like MoS$_2$ nano-stuffing electrochemically active. The ultra-thin 2D nano-sheets provide excellent cycle stability due to their neglectable volume changes during cycling. The 3D flower-like MoS$_2$-PrGO sandwich composites deliver high energy density, excellent conductivity and stable cyclic performance during charge-discharge process. With a nearly 100% coulombic efficiency, their reversible capacity is retained at 1,036 mA h g^{-1} even after 500 cycles at current densities of 100 mA g^{-1}. This novel design strategy provides a broad prospect for the development of advanced anode materials for superior lithium storage.

Keywords: molybdenum sulfide, graphene oxide, anode, composites, lithium ion batteries

INTRODUCTION

Lithium-ion batteries have become the main power source of portable electronic products because of their high energy density, long cycle life, and eco-friendliness (Dunn et al., 2011; Fan et al., 2019; Zhang et al., 2019). With the rapid development of mobile electronic devices and electric vehicles, the market has put forward higher requirements on the energy storage density and stability of batteries. Therefore, more attentions have been paid to the exploration of electrode materials with high capacity and advanced performance (Ding et al., 2019; Zhang et al., 2019).

Transition metal dichalcogenides (TMDs) have become a popular choice in the field of energy storage due to their graphene-like two-dimensional (2D) layered structure, in which lithium ions

tend to migrate among the 2D layers due to the weak van der Waals interactions (Yang et al., 2015; Cook et al., 2016; Wang et al., 2016). Among a variety of TMDs, MoS_2 is an ideal anode material for lithium ion batteries because its proper interlayer spacing endows this material a higher theoretical specific capacity (Kadam et al., 2019; Santhosha et al., 2019). However, its poor conductivity and large volume variations have limited its application as an advanced anode material. To address the above issues, MoS_2 has been engineered into different nanostructures and nanocomposites (Kadam et al., 2019; Santhosha et al., 2019; Sun et al., 2019; Wang M. et al., 2019; Wang Y. et al., 2019; Xie et al., 2019; Zhu et al., 2019). Recently, due to its excellent electrical, thermal and mechanical properties, graphene has been used to combine with MoS_2 to form an anode material for lithium-ion batteries (Huang et al., 2017; Tan et al., 2018; Anwer et al., 2019). The high mechanical strength and extraordinary conductivity of graphene greatly improve the structure stability and the electrical performance of the graphene-based MoS_2 nanocomposites. However, large volume changes occurred when lithium ions were embedded in the MoS_2 layers and preferentially interacted with S layers to form Li–S bonds. The significant capacity degradation triggered by the changes in MoS_2 volume still can not be eliminated. Moreover, the solid-electrolyte interphase (SEI) layer produced by organic electrolyte decomposition deforms and fractures during the expansion and contraction of MoS_2. The new SEI on the newly exposed MoS_2 surface results in low coulombic efficiency. The gradual accumulation of SEI further impedes the transfer of lithium ions. By self-assembling 2D MoS_2 nanosheets into three-dimensional (3D) layered porous nano-spheres with uneven surfaces, the capacity of the MoS_2 electrodes can be further improved. As we known, two-dimensional single-layer nanosheets are highly resistant to volume changes, while highly uneven surfaces ensure more active sites (Wang M. et al., 2013; Qi et al., 2018). It was predicted that the self-assembly of 3D hierarchical MoS_2 nano-flowers with open architecture will maximize the advantages of 2D MoS_2 nanosheets. Additionally, the conventional chemical exfoliation process will introduce oxygen functional groups to form a single layer of graphene oxide (GO). The loss of π system leads to a poor conductivity of GO. GO have to be reduced to the reduced GO (rGO) to reconstruct the sp2 hybridized network before binding to MoS_2. Although GO can be partially reduced through high-temperature annealing or chemical reduction, large aggregates are easily formed under van der Waals force. Moreover, MoS_2 nanostructures tend to separate from the rGO/GO surfaces due to the weak interaction between rGO/GO and MoS_2. Therefore, the assembly of micron-scale 3D hierarchical MoS_2 pore nanospheres on the surface of rGO nanosheets was a major challenge.

Herein, inspired by the structure of sandwiches, we constructed a novel 3D flower-like MoS_2-rGO sandwich nanocomposites (MoS_2-PrGO) for lithium-ion battery anode through a linking mode and *in-situ* conversion. Supported by the PEO chains, the enlarged interlayer space of rGO not only accommodated as many MoS_2 nano-flowers as possible, but also acted as a conductive framework. The mild volume expansion of the MoS_2 nano-flowers during charge-discharge

processes was effectively alleviated by the PEO chains. The rGO conductive framework mad all flower-like MoS_2 stuffings electrochemically active. With this unique design, the 3D flower-like MoS_2-PrGO sandwich composites exhibited remarkable specific capacity and ultra-stable cyclic performance during the electrochemical measurements.

EXPERIMENTAL METHOD

Preparation of Go

GO was prepared based on improved Hummers method. 1.5 g of potash nitrate ($NaNO_3$) and 3.0 g of flake graphite were dissolved in 100 mL of sulfuric acid (H_2SO_4, 98%), and stirred for 0.5 h under 10°C. Then, 10.0 g of potassium permanganate ($KMnO_4$) was slowly added to the mixture, followed by continuous magnetic stirring for 0.5 h. This mixture was diluted with 700 mL deionized water and continued to stir at 95°C for 1 h. Afterward, 30% hydrogen peroxide (H_2O_2, 15 mL) was dropped to the mixture and turned dark green solution into a bright yellow one. The suspension was then washed with 1:10 HCl solution and deionized water for several times. Finally, the obtained GO was freeze-dried for 48 h.

Preparation of MoS₂-PrGO

MoS_2@rGO was synthesized through one step hydrothermal method. Forty milligrams of rGO and 6.9 mg of PEO (Mw = 100,000) were dissolved in 60 ml of deionized water and homogenized by stirring for 12 h. After the addition of 200 mg of Sodium Molybdate Dihydrate ($Na_2MoO_4 \bullet 2H_2O$) and 500 mg of Sulfourea (NH_2CSNH_2), the mixture was stirred for 0.5 h and poured into 100 ml reactor to reacted at 210°C for 24 h. Naturally cooling to room temperature, the obtained products were washed with deionized water and ethanol for several times. The MoS_2/rGO nanocomposites were harvested after drying in vacuum at 60°C for 48 h.

Structure and Morphology Characterization

The phase purity of the synthesized products was examined by X-ray powder diffraction (XRD, Panalytical X' Pert, Holland) by using Cu-Ka radiation (λ = 1.5418 Å). The morphology of the products was characterized by field emission scanning electron microscopy (SEM, Model: JEOL JSM−7000F, Japan) and high-resolution transmission electron microscopy (HRTEM, Model: FEI Titan X 60–300, USA). X-ray photoelectron spectroscopy (XPS) measurements were performed on a Perkin-Elmer model PHI 5600 XPS system with a monochromated aluminum anode as the X-ray source.
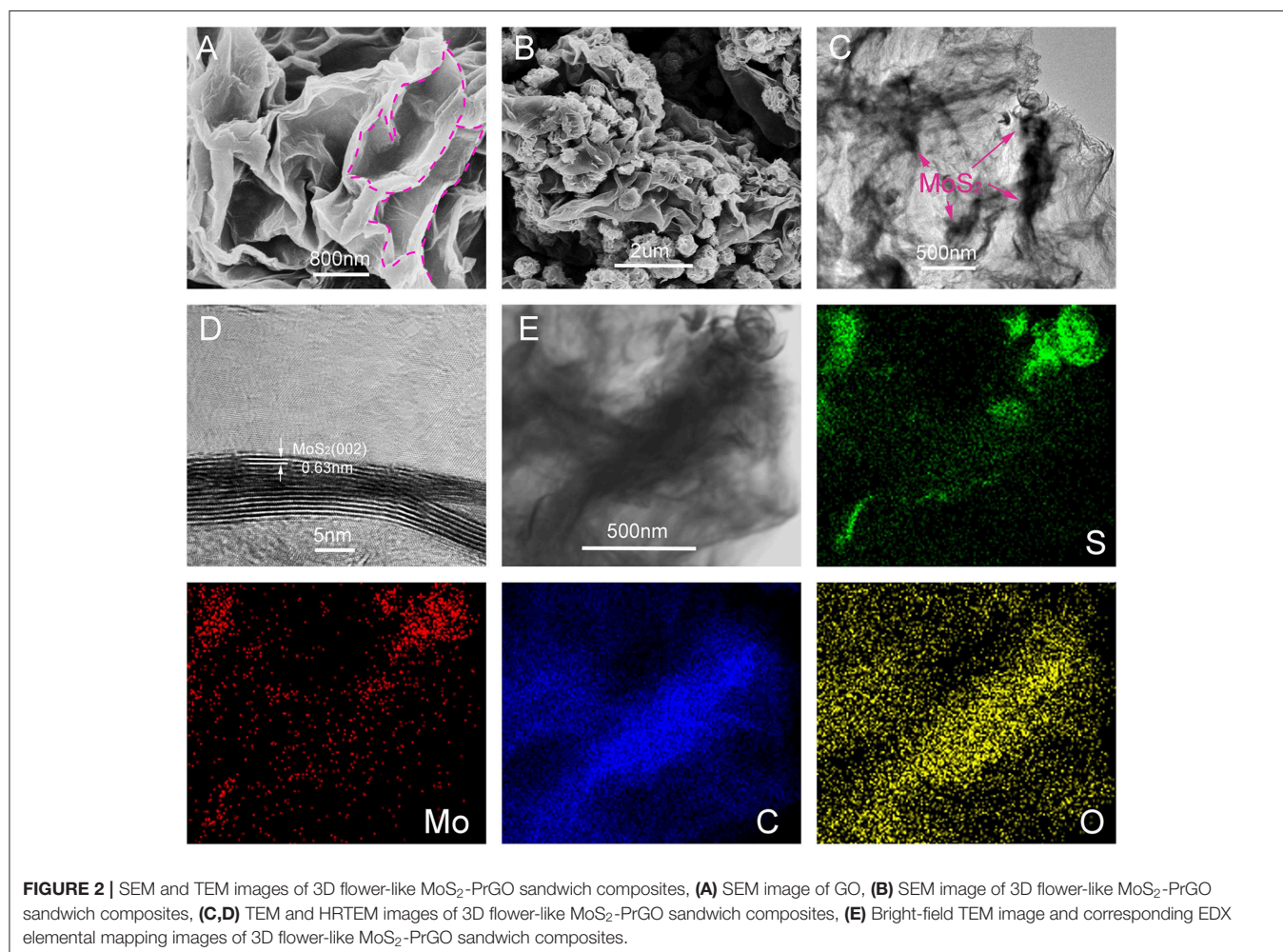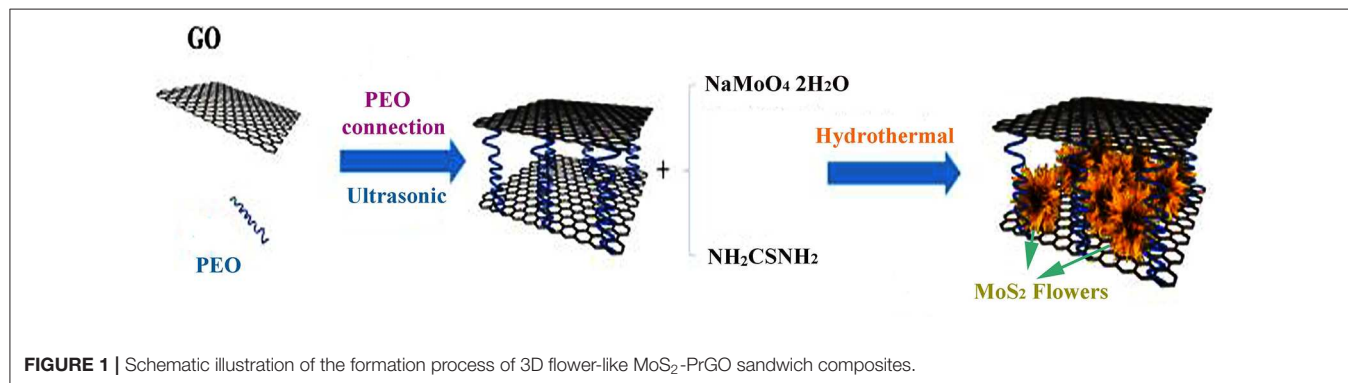
Electrochemical Measurements

Electrochemical tests were carried out in CR 2032 coin cells with lithium metal as the reference and counter electrode. Seventy percent active materials, 20% carbon black and 10 % PVDF were evenly mixed in N-methyl-2-pyrrolidone to form the cathode slurry. The active material loading was controlled at about 2 mg cm^{-2}. 1 M $LiPF_6$ in

ethylene carbonate and diethyl carbonate (V_{eth}: V_{die} 1:1) was used as electrolyte. Galvanostatic charge-discharge tests were performed by using a multichannel battery tester (Neware BTS-610) in a voltage window of 0–3.0 V. Cyclic voltammetry curves (CV) were carried out on a PARSTAT 4,000 electrochemical workstation at a scan rate of 0.2 mV s^{-1} in the range of 3.0–0.01 V(vs. Li/Li$^+$). Electrochemical impedance spectroscopy (EIS) was tested in the frequency range of 100 kHz−0.01 Hz.

RESULTS AND DISCUSSION

Synthesis and Characterization

Figure 1 illustrates the preparation mechanism of the 3D flower-like MoS_2-PrGO nanocomposites. Firstly, under the ultrasonic induction, PEO chains were tightly bound to the GO surface to form a large area of 3D PGO layered spatial structure due to the strong affinity between PEO's non-shared ether-oxygen electrons and GO hydrogen bonds. Secondly, under the electrostatic force,

FIGURE 1 | Schematic illustration of the formation process of 3D flower-like MoS_2-PrGO sandwich composites.

FIGURE 2 | SEM and TEM images of 3D flower-like MoS_2-PrGO sandwich composites, **(A)** SEM image of GO, **(B)** SEM image of 3D flower-like MoS_2-PrGO sandwich composites, **(C,D)** TEM and HRTEM images of 3D flower-like MoS_2-PrGO sandwich composites, **(E)** Bright-field TEM image and corresponding EDX elemental mapping images of 3D flower-like MoS_2-PrGO sandwich composites.
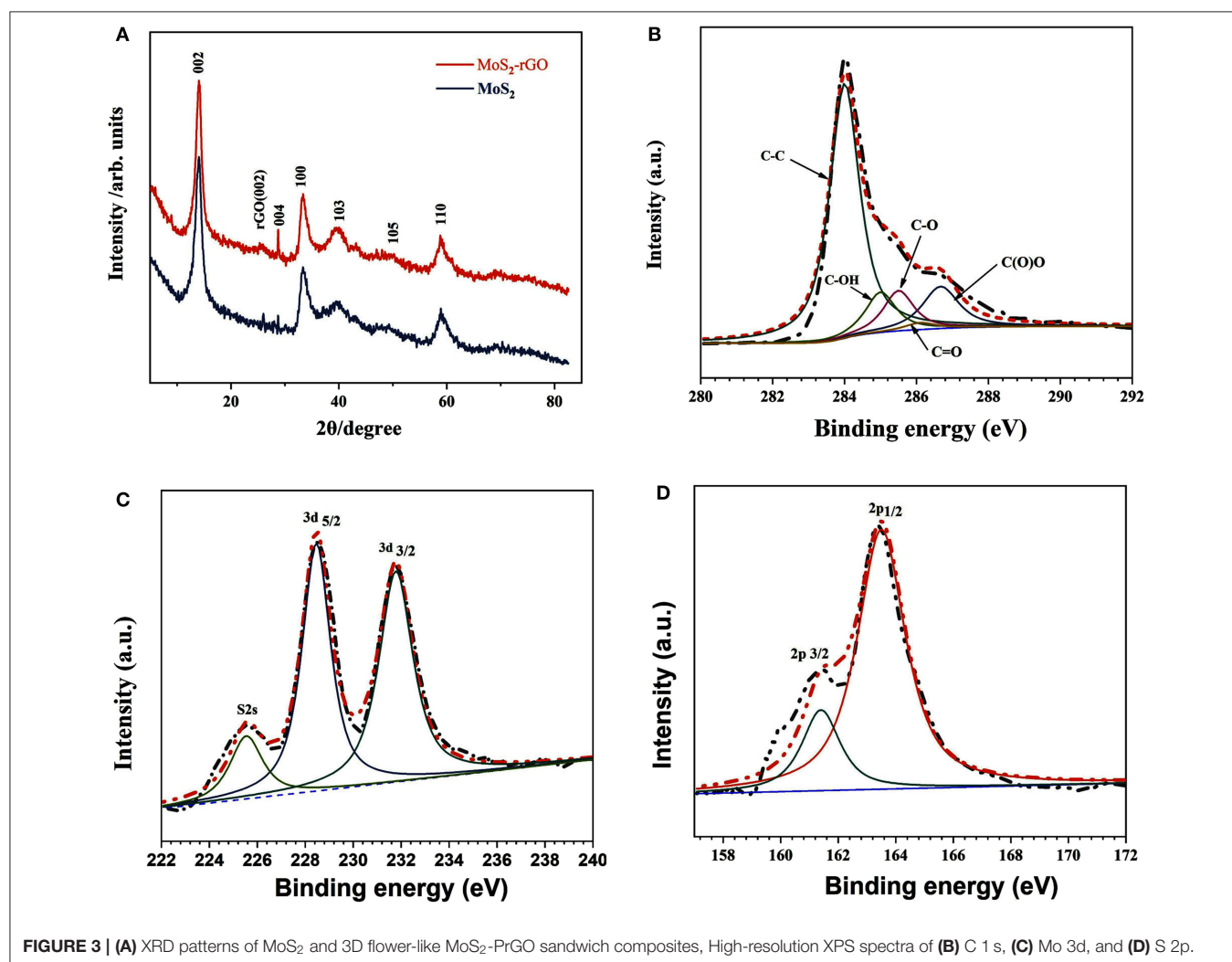
MoO_4^{2-} anions approached the GO surface and were mainly captured by the carboxyl, hydroxyl and epoxy groups (Chang and Chen, 2011). Finally, H_2S released by sulfourea converted MoO_4^{2-} and GO *in situ* to MoS_2 nano-flowers and rGO in the solvothermal process. Therefore, 3D flower-like MoS_2-PrGO sandwich nanocomposites were successfully obtained.

SEM and TEM were used to describe the morphology of the obtained sandwich nanocomposites. As shown in **Figure 2A**, the separated 2D ultrathin rGO nano-sheets were assembled into a remarkable 3D layered spatial structure under the linking of PEO. Supported by the PEO chains, the enlarged interlayer space can accommodate a significant number of micron-sized MoS_2 nano-flowers. **Figure 2B** shows the morphology of the 3D MoS_2-PrGO sandwich nanocomposites. The ultrathin MoS_2 nanosheets were assembled into distinct nano-flowers anchored on the surfaces of rGO hosts. The average size of MoS_2 nano-flowers was about 200 nm. The results of thermogravimetric analysis (TGA) indicates that the contents of MoS_2 in the obtained nanocomposites reached 83.3% (**Figure S1** and **Table S1**). This 3D layered sandwich structure is conducive to improve the

electronic and ionic conductivity. In addition, the PEO chains buffered the volume expansion of the MoS_2 nano-flowers during charge/discharge processes. The TEM image of the 3D layered MoS_2-PrGO sandwich nanocomposites (**Figure 2C**) reveals that the MoS_2 nano-flowers were well-encased in the rGO interlayers without aggregation, which is consistent with SEM image. The further HR-TEM image (**Figure 2D**) displays that the MoS_2 petals consisted of 5–10 monolayers. The interlayer distance between each monolayer was about 0.62 nm, corresponding to the (002) lattice planes of MoS_2 (Lin et al., 2017). The corresponding EDX mapping of C, O, S, and Mo reveals that the C and O elements were homogeneously distributed in the specimens (**Figure 2E**), while the S and Mo elements were agglomerated with remarkable flower-liked hot spots. This further confirmed that the ultrathin MoS_2 nanosheets were assembled into nano-flowers anchored on the surfaces of rGO hosts, successfully forming a 3D flower-like MoS_2-PrGO sandwich architecture.

Figure 3A presents the XRD pattern of the 3D flower-like MoS_2-PrGO sandwich composites and the commercial MoS_2

FIGURE 3 | (A) XRD patterns of MoS_2 and 3D flower-like MoS_2-PrGO sandwich composites, High-resolution XPS spectra of **(B)** C 1 s, **(C)** Mo 3d, and **(D)** S 2p.
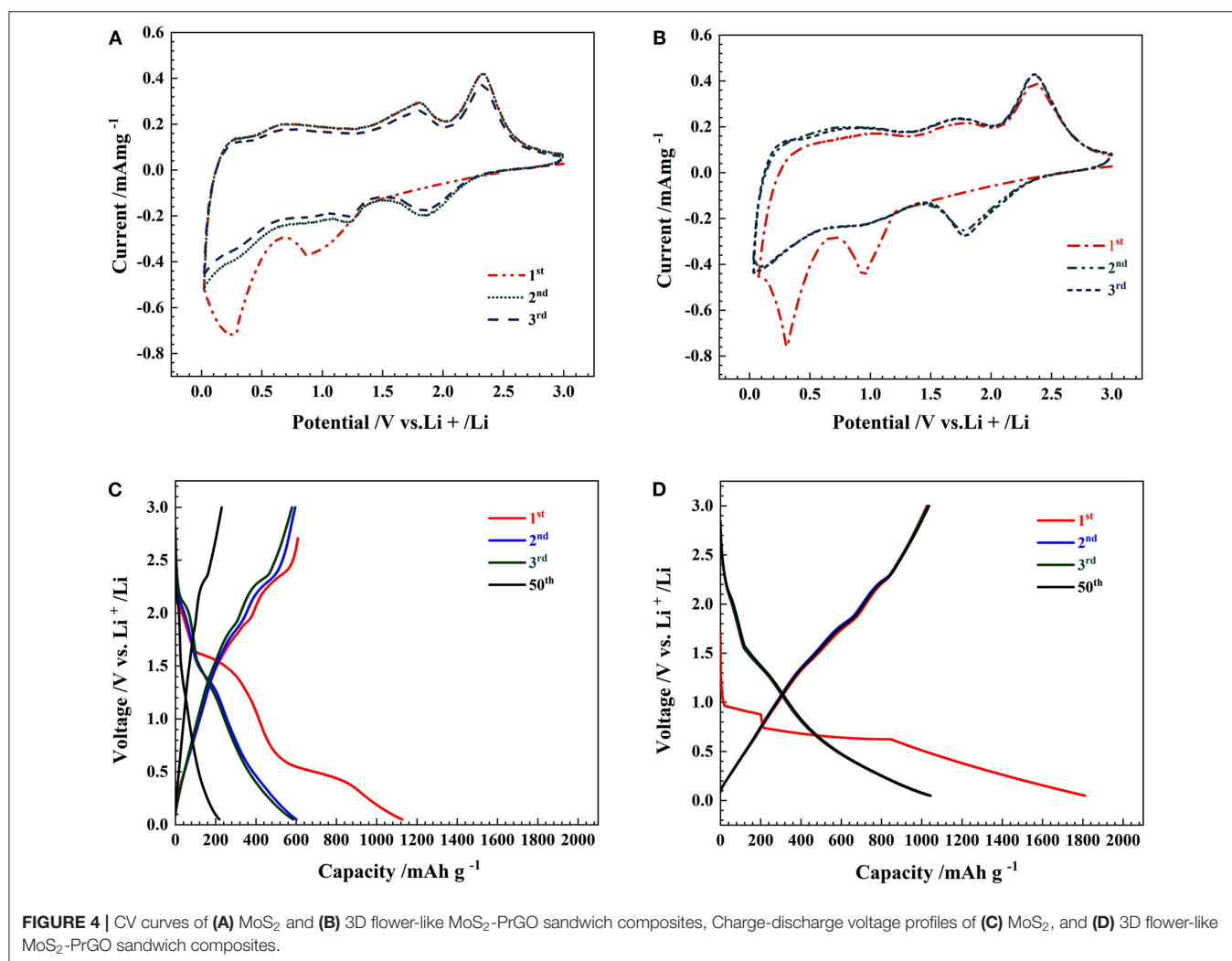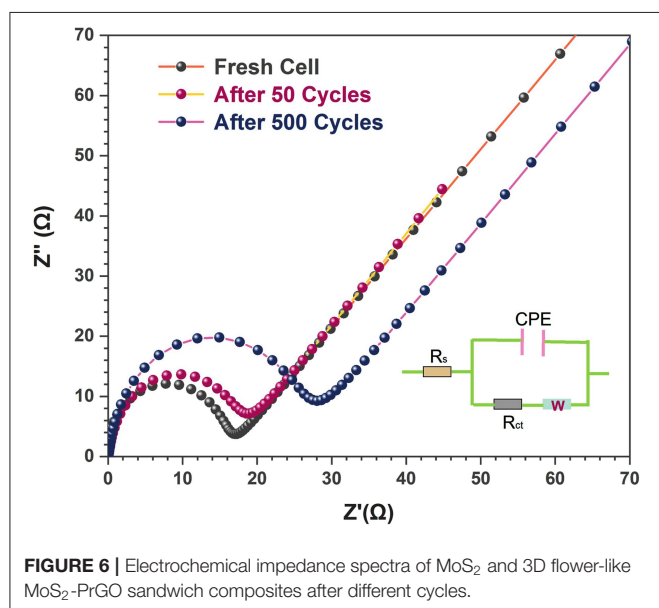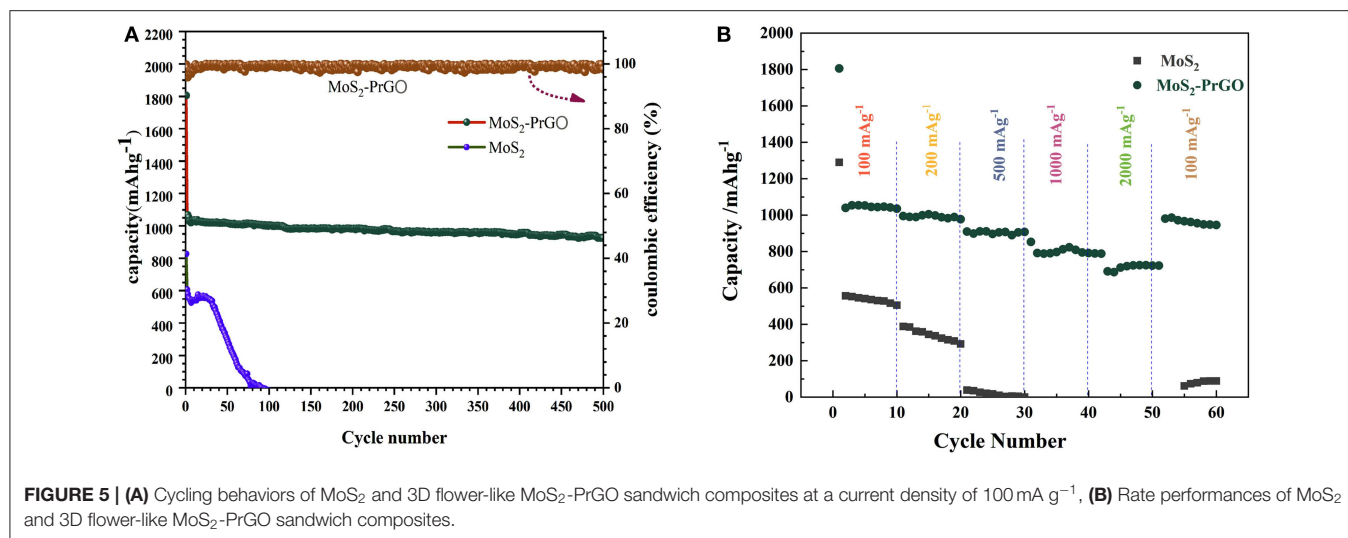
specimens. All diffraction peaks of the MoS_2 matched well the diffraction peaks of the typical hexagonal MoS_2 (JCPDS 37-1492). The obtained hexagonal MoS_2 had lattice parameters of $a = b = 3.16$ Å and $c = 12.31$ Å, which were consisted with the experimental values (Guo et al., 2017). Other than diffraction peaks of the hexagonal MoS_2, a weak and broad peak appeared in the XRD pattern of the 3D flower-like composites. This additional peak located at 24.5° was attributed to the (002) planes of rGO hosts (He et al., 2014; Chong et al., 2017). The chemical bonding conditions of the 3D flower-like composites were further analyzed by XPS. As shown in **Figure 3B**, XPS spectrum of the C 1 s core-level was divided into two deconvolution peaks. The intense peak located at around 284.6 eV matched the C–C bonds of rGO nanosheets, and the weak peak near 286.0 eV was contributed by C–O bond (Yang et al., 2009). **Figures 3C,D** show the XPS spectra of Mo 3d and S 2p, respectively. The bonding peaks centered at 228.8 and 232.1 eV reflected the bonding states of Mo $3d_{5/2}$ and Mo $3d_{3/2}$, implying a standard Mo^{4+} state. The main and satellite peaks of S 2p spectrum were, respectively, located at 161.7 and

162.8 eV with a 1.1 eV energy separation, corresponding to the S^{2-} state (Khawula et al., 2016). The XPS analysis indicated that S and Mo elements in the final products existed in the form of MoS_2.
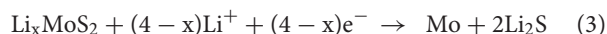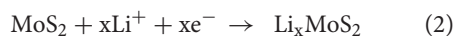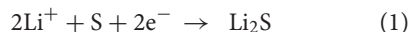
Electrochemical Properties

Figures 4A,B illustrate the first three cyclic CV curves of the commercial MoS_2 specimens and the 3D flower-like MoS_2-PrGO sandwich composites. In the first cathodic scan, the CV curves of the commercial MoS_2 specimens and the 3D flower-like composites exhibited two significant reduction peaks at ~0.88 and 0.26 V. The reduction peak at 0.88 V was derived from the formation of Li_xMoS_2 after lithium ions were inserted into (002) plane of MoS_2 (Liu et al., 2015), while the other peak at 0.26 V was induced by the conversion of MoS_2 into Mo and Li_2S. The anodic scan peak around 2.39 V reflected the reaction of Li_2S into Li^+ and S. Over the next two cycles, both CV curves displayed an additional reduction peak near 1.86 V. This additional reduction peak was mainly attributed to the formation of gelatinous polymeric layers (Du et al., 2010). The

FIGURE 4 | CV curves of **(A)** MoS_2 and **(B)** 3D flower-like MoS_2-PrGO sandwich composites, Charge-discharge voltage profiles of **(C)** MoS_2, and **(D)** 3D flower-like MoS_2-PrGO sandwich composites.

FIGURE 5 | (A) Cycling behaviors of MoS$_2$ and 3D flower-like MoS$_2$-PrGO sandwich composites at a current density of 100 mA g^{-1}, **(B)** Rate performances of MoS$_2$ and 3D flower-like MoS$_2$-PrGO sandwich composites.

FIGURE 6 | Electrochemical impedance spectra of MoS$_2$ and 3D flower-like MoS$_2$-PrGO sandwich composites after different cycles.

electrochemical reaction mechanism of each peak was written as (Wang Z. et al., 2013).

$$2Li^+ + S + 2e^- \rightarrow Li_2S \qquad (1)$$

$$MoS_2 + xLi^+ + xe^- \rightarrow Li_xMoS_2 \qquad (2)$$

$$Li_xMoS_2 + (4-x)Li^+ + (4-x)e^- \rightarrow Mo + 2Li_2S \quad (3)$$

Compared with the commercial MoS$_2$ specimens, the CV curves of the 3D flower-like composites presented stronger reduction peaks because the electrochemical reaction of lithium with MoS$_2$ was synchronous with that of lithium with rGO (Wang and Li, 2007).

Figures 4C,D show the charge-discharge voltage profiles of the commercial MoS$_2$ specimens and the 3D flower-like MoS$_2$-PrGO sandwich composites at a constant current density of 100 mA g^{-1}. During the first discharge, the commercial MoS$_2$ anode produced two potential plateaus at 1.4 and 0.5 V. The plateau at 1.4 V corresponded to the formation of Li$_x$MoS$_2$ lattice and the insertion of lithium ions. The discharge plateau at 0.5 V was attributed to the conversion of MoS$_2$ into Mo and Li$_2$S, as well as the formation of gelatinous polymeric layers driven by electrochemical degradation of electrolyte (Ding et al., 2011). Consistent with CV test results, the broad plateau at about 2.3 V was a trace of the Li$_2$S decomposition. As shown in **Figure 4D**, although those plateaus recurred in the charge-discharge voltage profiles of the 3D flower-like composites, their width decreased. This indicated that the electron migration rate of the 3D flower-like composites is faster than that of the commercial MoS$_2$ specimens. Furthermore, the gentle potential curve slope and large charge capacity indicate that the 3D flower-like composites delivered more reactive sites and nice cycle stability. The first discharge-charge capacities of the 3D flower-like composites were 1,800 and 1,122 mA h g^{-1}, respectively, far higher than those of the commercial MoS$_2$ specimens. The initial irreversible capacity loss was about 37.7 %, mainly caused by the lithium ion residues in the MoS$_2$ lattice and the formation of SEI films (Tang et al., 2009).

Figure 5A plots the cycling performances of the commercial MoS$_2$ specimens and the 3D flower-like MoS$_2$-PrGO sandwich composites at a constant current density of 100 mA g^{-1}. It was obvious that the commercial MoS$_2$ electrodes could not afford prolonged cycling and rapidly decayed to zero after 170 cycles, while the 3D flower-like composites exhibited extraordinary cycling behavior and still maintained a reversible capacity of 1,036 mA h g^{-1} after 500 cycles. SEM test results reveals that after 500 cycles, the structure of the 3D flower-like composites was still intact without obvious pulverization (**Figure S2**). The high reversible capacity and remarkable cycling behavior of the 3D flower-like composites were also reflected in the rate

performance. **Figure 5B** shows the rate cycling behavior of the commercial MoS_2 specimens and the 3D flower-like MoS_2-PrGO sandwich composites at various current densities of 100–2,000 mA g^{-1}. Compared with the commercial MoS_2 specimens, the 3D flower-like composites presented an excellent rate performance. Their specific capacity remained at 579 mA h g^{-1} when current density continuously increased to 2,000 mA g^{-1}. In contrast, commercial MoS_2 specimens failed completely before the cycling current increased to 500 mA g^{-1}. In addition, when the current density changed to 100 mA g^{-1}, the specific capacity of the 3D flower-like composites almost returned to their initial value, and remained stable throughout the subsequent cycling.

The excellent electrochemical performance of the 3D flower-like composites was further verified by the EIS measurements. **Figure 6** shows the Nyquist plots of the 3D flower-like composite electrodes after different cycles. All Nyquist plots were semi-circular at the high frequencies and oblique in the low frequencies. The semicircle reflected the charge-transfer impedance on electrode (R_{ct}), and the slope line in the low-frequency range represented the Warburg impedance (W) associated with the diffusion process of lithium ions (Xu et al., 2013). The Randles equivalent circuit inserted in **Figure 6** simulated the corresponding electrochemical system, where CPE represents the double-layer capacitance and Rs is the ohmic resistance. The fresh 3D flower-like composite electrodes exhibited a small semi-circular with a slight increase after 500 cycles. This indicated that the 3D flower-like composite electrodes possessed lower charge-transfer resistance and long-term cycling stability. Their lower charge-transfer resistance is due to the good conductivity of rGO. Furthermore, their unique 3D layered sandwich structure also facilitates rapid transfer of lithium ions upon cycling. Assisted by PEO chains buffering, the robust rGO interlayers effectively suppressed the volume expansion of MoS_2 and ensured a good cycling performance. In addition, the ultrathin MoS_2 nanosheets also accommodated a high tolerance to structure changes. Their unique 3D flower-like sandwich structure provided more active sites for the interface reaction between active materials and the lithium-ions, which endowed the final electrodes with a high reversible capacity.

CONCLUSIONS

In summary, the 3D flower-like MoS_2-PrGO sandwich composites were synthesized by a facile hydrothermal method.

PEO with non-shared ether-oxygen electron pairs firstly bridged the separated 2D ultrathin rGO nano-sheets into a remarkable 3D layered spatial structure, and then the MoS_2 nano-flowers were homogeneously grown on the surfaces of rGO hosts by *in-situ* conversion. This unique 3D flower-like sandwich structure has more active sites and large volume change accommodation. The 3D flower-like composites highlighted high energy density and remarkable cycling stability, and excellent conductivity. Their discharge capacity was retained at 1036 mA h g^{-1} even after 500 cycles at current densities of 100 mA g^{-1}. This novel structure design of anode material provides new ideas for improving the electrochemical performances of other metal sulfides.

DATA AVAILABILITY STATEMENT

All datasets generated for this study are included in the article/**Supplementary Material**.

AUTHOR CONTRIBUTIONS

YZha conducted the experiments. ZZ was the supervisor of this research work. YZha, HZ, ZZ, and SX helped with writing. YZha, YZho, and YW performed the characterization and data analysis. All authors involved the analysis of experimental data and manuscript preparation.

FUNDING

ACKNOWLEDGMENTS

SUPPLEMENTARY MATERIAL

The Supplementary Material for this article can be found online at: https://www.frontiersin.org/articles/10.3389/fchem.2020.00094/full#supplementary-material

REFERENCES

Anwer, S., Huang, Y., Li, B., Govindan, B., Liao, K. J., Cantwell, W., et al. (2019). Nature-inspired, graphene-wrapped 3D MoS_2 ultrathin microflower architecture as a high-performance anode material for sodium-ion batteries. *ACS Appl. Mater. Interf.* 11, 22323–22331. doi: 10.1021/acsami.9b04260

Chang, K., and Chen, W. (2011). *In situ* synthesis of MoS_2/graphene nanosheet composites with extraordinarily high electrochemical performance for lithium ion batteries. *Chem. Commun.* 47, 4252–4254. doi: 10.1039/c1cc10631g

Chong, W. G., Huang, J., Xu, Z., Qin, X., Wang, X., and Kim, J. K. (2017). Lithium-sulfur battery cable made from ultralight, flexible graphene/carbon nanotube/sulfur composite fibers. *Adv. Funct. Mater.* 27, 1604815–1604824. doi: 10.1002/adfm.201604815

Cook, J. B., Kim, H. S., Yan, Y., Ko, J. S., Robbennolt, S., Dunn, B., et al. (2016). Mesoporous MoS_2 as a transition metal dichalcogenide exhibiting pseudocapacitive Li and Na-ion charge storage. *Adv. Energy Mater.* 6:1501937. doi: 10.1002/aenm.201501937

Ding, J., Zhang, H., Zhou, H., Feng, J., Zheng, X., Zhong, C., et al. (2019). Sulfur-grafted hollow carbon spheres for potassium-ion battery anodes. *Adv. Mater.* 31:1900429. doi: 10.1002/adma.201900429

Ding, S., Chen, J. S., and Lou, X. W. (2011). Glucose-assisted growth of MoS_2 nanosheets on CNT backbone for improved lithium storage

properties. *Chem. Eur. J.* 17, 13142–13145. doi: 10.1002/chem.20110
2480

Du, G., Guo, Z., Wang, S., Zeng, R., Chen, Z., and Liu, H. (2010). Superior stability
and high capacity of restacked molybdenum disulfide as anode material for
lithium ion batteries. *Chem. Commun.* 46, 1106–1108. doi: 10.1039/B920277C

Dunn, B., Kamath, H., and Tarascon, J. M. (2011). Electrical energy storage for the
grid: a battery of choices. *Science* 334, 928–935. doi: 10.1126/science.1212741

Fan, X., Liu, X., Hu, W., Zhong, C., and Lu, J. (2019). Advances in the
development of power supplies for the internet of everything. *InfoMat* 1,
130–139. doi: 10.1002/inf2.12016

Guo, P., Liu, D., Liu, Z., Shang, X., Liu, Q., and He, D. (2017). Dual
functional MoS_2/graphene interlayer as an efficient polysulfide barrier
for advanced lithium-sulfur batteries. *Electrochim. Acta.* 256, 28–36.
doi: 10.1016/j.electacta.2017.10.003

He, G., Hart, C. J., Liang, X., Garsuch, A., and Nazar, L. F. (2014). Stable cycling of
a scalable graphene-encapsulated nanocomposite for lithium-sulfur batteries.
ACS Appl. Mater. Interf. 6, 10917–10923. doi: 10.1021/am500632b

Huang, H., Huang, J., Liu, W., Fang, Y., Liu, Y., and Huang, H., et al. (2017).
Ultradispersed and single-layered MoS_2 nanoflakes strongly coupled with
graphene: an optimized structure with high kinetics for the hydrogen evolution
reaction. *ACS Appl. Mater. Interf.* 9, 39380–39390. doi: 10.1021/acsami.7b12038

Kadam, S. R., Kawade, U. V., Bar-Ziv, R., Gosavi, S. W., Bar-Sadan, M., and Kale,
B. B. (2019). Porous MoS_2 framework and its functionality for electrochemical
hydrogen evolution reaction and lithium ion batteries. *ACS Appl. Energy Mater.*
2, 5900–5908. doi: 10.1021/acsaem.9b01045

Khawula, T. N. Y., Raju, K., Franklyn, P. J., Sigalas, I., and Ozoemena, K. I. (2016).
Symmetric pseudocapacitors based on molybdenum disulfide (MoS_2)-modified
carbon nanospheres: correlating physicochemistry and synergistic interaction
on energy storage. *J. Mater. Chem. A* 4, 6411–6425. doi: 10.1039/C6TA00114A

Lin, H., Yang, L., Jiang, X., Li, G., Zhang, T., Yao, Q., et al. (2017). Electrocatalysis of
polysulfide conversion by sulfur-deficient MoS_2 nanoflakes for lithium-sulfur
batteries. *Energy Environ. Sci.* 10, 1476–1486. doi: 10.1039/C7EE01047H

Liu, G., Feng, Y., Li, Y., Qin, M., An, H., Hu, W., et al. (2015). Three-
dimensional multilayer assemblies of MoS_2/reduced graphene oxide for high-
performance lithium ion batteries. *Part. Part. Syst. Charact.* 32, 489–497.
doi: 10.1002/ppsc.201400207

Qi, X., Zhang, H., Zhang, Z., Bian, Y., Shen, A., Xu, P., et al. (2018). Subunits
controlled synthesis of three-dimensional hierarchical flowerlike a-Fe_2O_3
hollow spheres as high-performance anodes for lithium ion batteries. *Appl.
Surf. Sci.* 452, 174–180. doi: 10.1016/j.apsusc.2018.04.253

Santhosha, A. L., Nayak, P. K., Pollok, K., Langenhorst, F., and Adelhelm, P.
(2019). Exfoliated MoS_2 as electrode for all-solid-state rechargeable lithium-ion
batteries. *J. Phys. Chem. C* 123, 12126–12134. doi: 10.1021/acs.jpcc.9b01816

Sun, D., Huang, D., Wang, H., Xu, G. L., Zhang, X., Zhang, R., et al. (2019). 1T
MoS_2 nanosheets with extraordinary sodium storage properties via thermal-
driven ion intercalation assisted exfoliation of bulky MoS_2. *Nano Energy* 61,
361–369. doi: 10.1016/j.nanoen.2019.04.063

Tan, L., Li, X., Wang, Z., Guo, H., and Wang, J. (2018). Lightweight
reduced graphene oxide@MoS_2 interlayer as polysulfide barrier for high-
performance lithium-sulfur batteries. *ACS Appl. Mater. Interf.* 10, 3707–3713
doi: 10.1021/acsami.7b18645

Tang, L., Wang, Y., Li, Y., Feng, H., Lu, J., and Li, J. (2009). Preparation
structure, and electrochemical properties of reduced graphene sheet
films. *Adv. Funct. Mater.* 19, 2782–2789. doi: 10.1002/adfm.20090
0377

Wang, M., Li, G., Xu, H., Qian, Y., and Yang, J. (2013). Enhanced lithium storage
performances of hierarchical hollow MoS_2 nanoparticles assembled from
nanosheets. *ACS Appl. Mater. Interf.* 5, 1003–1008. doi: 10.1021/am3026954

Wang, M., Xu, Y. H., Lu, F., Zhu, Z., Dong, J. Y., Fang, D. L., et al. (2019).
Enhanced Li-ion-storage performance of MoS_2 through multistage structural
design. *ChemElectroChem* 6, 475–1484. doi: 10.1002/celc.201801533

Wang, Q., and Li, J. (2007). Facilitated lithium storage in MoS_2 overlayers
supported on coaxial carbon nanotubes. *J. Phys. Chem. C.* 111, 1675–1682
doi: 10.1021/jp066655p

Wang, Y., Wei, R., Zhang, B., Lv, H., Xu, D., Hao, Q., et al. (2019). Template-
assisted self-sulfuration formation of MoS_2 nanosheets embedded in ordered
mesoporous carbon for lithium storage. *ACS Appl. Energy Mater.* 2, 6158–6162.
doi: 10.1021/acsaem.9b01262

Wang, Y., Yu, L., and Lou, X. W. (2016). Synthesis of highly uniform
molybdenum-glycerate spheres and their conversion into hierarchical mos_2
hollow nanospheres for lithium-ion batteries. *Angew. Chem. In. Edit.* 55,
7423–7426. doi: 10.1002/anie.201601673

Wang, Z., Chen, T., Chen, W., Chang, K., Ma, L., Huang, G., et al. (2013). CTAB-
assisted synthesis of single-layer MoS_2-graphene composites as anode materials
of Li-ion batteries. *J. Mater. Chem. A* 1, 2202–2210. doi: 10.1039/C2TA00598K

Xie, H., Chen, M., and Wu, L. (2019). Hierarchical nanostructured
NiS/MoS_2/C composite hollow spheres for high performance sodium-
ion storage performance. *ACS Appl. Mater. Interf.* 11, 41222–41228.
doi: 10.1021/acsami.9b11078

Xu, J., Wang, Q., Wang, X., Xiang, Q., Liang, B., Chen, D., et al.
(2013). Flexible asymmetric supercapacitors based upon Co_9S_8
nanorod//Co_3O_4@RuO_2 nanosheet arrays on carbon cloth. *ACS Nano.* 7,
5453–5462. doi: 10.1021/nn401450s

Yang, D., Velamakanni, A., Bozoklu, G., Park, S., Stoller, M., Piner, R., et al. (2009).
Chemical analysis of graphene oxide films after heat and chemical treatments
by X-ray photoelectron and micro-raman spectroscopy. *Carbon* 47, 145–152.
doi: 10.1016/j.carbon.2008.09.045

Yang, E., Ji, H., and Jung, Y. (2015). Two-dimensional transition metal
dichalcogenide monolayers as promising sodium ion battery anodes. *J. Phys.
Chem. C* 119, 26374–26380. doi: 10.1021/acs.jpcc.5b09935

Zhang, Z., Xu, P., Zhang, H., Shen, A., and Zhao, Y. (2019). Flexible
three-dimensional titanium-dioxide-based hollow nanoflower arrays for
advanced lithium-ion battery anodes. *ACS Appl. Energy Mater.* 2, 5744–5752.
doi: 10.1021/acsaem.9b00869

Zhu, Z., Tang, Y., Leow, W. R., Xia, H., Lv, Z., Wei, J., et al. (2019).
Approaching the lithiation limit of MoS_2 while maintaining its layered
crystalline structure to improve lithium storage. *Angew. Chem. In. Edit.* 58,
3521–3526. doi: 10.1002/anie.201813698